frontiers | Frontiers in Earth Science

TYPE Original Research
PUBLISHED 30 August 2024
DOI 10.3389/feart.2024.1454629

Check for updates

OPEN ACCESS

EDITED BY
Wen Nie,
Jiangxi University of Science and Technology, China

REVIEWED BY
Jing Bi,
Guizhou University, China
Shaojun Li,
Chinese Academy of Sciences (CAS), China
Feng Shan,
University of Technology Sydney, Australia

*CORRESPONDENCE
Chunmei Chu,
ccmdkxy@xju.edu.cn
Longwei Yang,
yang0504@chd.edu.cn

RECEIVED 25 June 2024
ACCEPTED 14 August 2024
PUBLISHED 30 August 2024

CITATION
Chu C, Yang L, Cheng W, Wang J and Wang X (2024) Triaxial mechanical behaviours of Ili loess after freeze–thaw.
Front. Earth Sci. 12:1454629.
doi: 10.3389/feart.2024.1454629

COPYRIGHT
© 2024 Chu, Yang, Cheng, Wang and Wang. This is an open-access article distributed under the terms of the Creative Commons Attribution License (CC BY). The use, distribution or reproduction in other forums is permitted, provided the original author(s) and the copyright owner(s) are credited and that the original publication in this journal is cited, in accordance with accepted academic practice. No use, distribution or reproduction is permitted which does not comply with these terms.

Triaxial mechanical behaviours of Ili loess after freeze–thaw

Chunmei Chu[1,2]*, Longwei Yang[3]*, Wenyu Cheng[1], Juncheng Wang[1] and Xiang Wang[1]

[1]School of Geological and Mining Engineering, Xinjiang University, Urumqi, China, [2]School of Geology Engineering and Geomatics, Chang'an University, Xi'an, China, [3]Wuhan Design & Research Institute Co., Ltd. of China Coal Technology and Engineering Group, Wuhan, China

Loess is strongly sensitive to water, and its properties are substantially affected by weathering and other factors. Loess landslides, which are widely distributed in Ili, are closely related to seasonal freeze–thaw effects. In this study, multiple freeze–thaw cycle tests were conducted on loess samples with different moisture contents from the Ili region, and triaxial shear tests were conducted to study mechanical characteristics of the loess. Variations in the microstructure of the loess samples were analysed using scanning electron microscopy images to reveal the underlying mechanisms. The results showed that the freeze–thaw cycles significantly influence failure mode of the stress–strain curve of loess samples with a lower moisture content of 10%, which transitioned from strain softening to strain hardening with six cycles as the turning point, whereas the stress–strain curve transitioned from strong to weak hardening for the loess samples with higher moisture content of 18%. As the number of freeze–thaw cycles increased, failure strength and shear strength parameters of loess gradually decreased, and tended to stabilize after the 10th cycle. In addition, strength parameters deterioration is most significant after the first cycle, and the degree of cohesion deterioration was much greater than that of internal friction angle. Cohesion and internal friction angle showed attenuation exponential function and polynomial function relationship, respectively, with the number of freeze–thaw cycles, and their fitting parameters underwent a sudden change with increasing moisture content, with 14% as the turning point. Microscopic SEM revealed that the number of overhead pores increased, and point–to–point contact between particles increased after freeze–thaw, which was consistent with increase in of loess porosity. This revealed the fundamental reason for the significant deterioration in loess strength caused by freeze–thaw cycles.

KEYWORDS

Ili loess, freeze-thaw cycle, failure mode, shear strength parameters, deterioration degree, Microstructure

1 Introduction

Loess is a special type of loose sediment formed during the Quaternary with porous pores and weak cementation. Its composition is mainly dominated by silty particles with unique microstructural characteristics (Hu et al., 2021). It is strongly sensitive to water and its properties are substantially affected by weathering and other factors. Loess is widely distributed in the northwestern region of China, Ili located the Tianshan Mountains, is the westernmost part of China's loess distribution area and is a typical seasonally frozen soil region (Zhuang et al., 2021). The rising temperature in spring leads to thawing of frozen loess, resulting in frequent occurrences of loess landslides, such as the super large Gallente,

the Yining Kizilesai, and the Zeketai landslides in the Ili Valley which mainly occur in spring and summer. (Wang and Yao, 2003). highlighted that seasonal freeze–thaw cycles are the main factor causing loess landslides. Under the cyclic action of climate change, the soil is in a state of repeated freezing and melting with its strength gradually deteriorating, easily leading to the occurrence of geological disasters (Zhou et al., 2018; Kong et al., 2023; Liu et al., 2020; Ismeik and Shaqour, 2020; Nguyen et al., 2019; Xu et al., 2018; Bragar et al., 2022; Liu et al., 2023; Jing et al., 2022; Zhou et al., 2023). Zhuang et al. (2021) highlighted that loess landslides in the Ili Basin are strongly affected by seasonal freeze–thaw cycles. Therefore, in the context of construction of "the Belt and Road," studying on the mechanical properties of the Ili loess under the freeze–thaw effect in the seasonal freezing area is particularly important.

With increase in engineering construction in western China, studying mechanical properties of loess under freeze–thaw conditions has become an important issue in the cold regions. Through laboratory experiments in recent years, most researchers have found that repeated freeze–thaw cycles weaken the strength of loess, and the variation law of loess shear strength is affected by many factors, such as moisture content, porosity, dry density, plasticity index, stress, freeze–thaw cycles, and temperature (Xu et al., 2018; Wang et al., 2018; Xu et al., 2018; Liu et al., 2021; Wang et al., 2024). Similar conclusions have been reached for variation of cohesion (one of the shear strength parameters) with the number of freeze–thaw cycles, and the cohesion of loess is strongly deteriorated by the effect of freeze–thaw cycles, which decreases to the lowest value after a certain number of freeze–thaw cycles (Wang et al., 2024; Ni and Shi, 2014; Ye et al., 2018). However, results of the freeze–thaw effect on the internal friction angle (the other shear strength parameter) were different. Some researchers have found that there is no significant change in internal friction angle (Xu et al., 2018; Song et al., 2008; Dong et al., 2010), while some researchers have obtained that internal friction angle slightly increases with the total number of freeze–thaw cycles (Song et al., 2008; Wang et al., 2024; Ye et al., 2018; Liu et al., 2021). Some scholars have also found that freeze–thaw cycles have a significant weakening effect on cohesion of highly saturated loess (Qian, 2018). For experimental studies on shear strength parameters, from previous simple direct shear tests to current more realistic triaxial shear tests, triaxial shear tests have been increasingly applied due to various advantages (Zhou et al., 2018; Kong et al., 2023; Wang et al., 2018; Li et al., 2018; Ren and Vanapalli, 2020; Yin et al., 2022; Zhang et al., 2024).

Macroscopic engineering properties of soil are significantly influenced its microstructural state and variation laws (Hong and Liu, 2010). Therefore, increasing number of scholars focus on revealing the mechanism of mechanical properties variation of loess under various weathering effects and loadings from microstructure perspective (Gao, 2013; Mu et al., 2011; Wang et al., 2016; Wei and Li, 2019; Zhang et al., 2020; Liang et al., 2023; Ye and Li, 2019; Hu et al., 2022; Nie et al., 2023). Several studies have found that freeze–thaw cycles cause changes in the micro–structure of loess, such as particle size distribution, roundness, contact mode, cementation, pore area, size, and type, etc. After freeze–thaw, large particles in loess are decomposed into several small particles, the fine particles increase, angularity of the particle surface is continuously rounded, and cementation of soil deteriorated (Xu et al., 2018; Ye et al., 2018; Qian, 2018). Ni and Shi (2014) illustrated through scanning electron microscopy (SEM) experiments that continuous decrease in cohesion was caused by repeated freeze–thaw, which gradually weakened the original inherent cementation between loess particles. Ye and Li (2019) analysed changes in the structure of loess under freeze–thaw cycles, and highlighted that with increase in the number of freeze–thaw cycles, contact between particles changes from surface–plane contact to point–plane and point–point contact, and porosity ratio of the cross–section increases with the increase in freeze–thaw cycles (Ye et al., 2020; Li et al., 2020; Liu et al., 2021).

In recent years, there has been more research on Ili loess, with most studies focusing on collapsibility, water retention, the influence of soluble salt content on mechanical properties, and the tensile properties (An et al., 2018; Liu et al., 2021; Wang et al., 2019; Niu et al., 2021; Zheng et al., 2022). With the continuous increase of loess landslides in Ili region, through on–site investigations, remote sensing and other methods, many scholars have conducted study on movement process and formation mechanism of landslides and found that these are closely related to seasonal freeze–thaw effects and rainfall (Zhuang et al., 2021; Li et al., 2020; Liu et al., 2021; Yu et al., 2022). Actually, the decrease in soil strength is the core factor causing landslides, which has been confirmed by many scholars (Zhuang et al., 2021; Zhang et al., 2022; Bragar et al., 2022; Liu et al., 2023; Wang et al., 2024). However, there is little attention paid to the study on effect of freeze–thaw on Ili loess deterioration, which is an important factor contributing to the formation of loess landslides. Therefore, further research focusing on the deterioration of mechanical properties and micro–mechanisms of Ili loess under freeze–thaw action is needed to better study the mechanism of landslides formation in seasonally frozen soil region from both macro and micro perspectives.

Here, we aimed to study on the macroscopic characteristics including the failure mode and the variation law of loess strength under freeze–thaw cycles, and explore the deterioration mechanism of loess strength under freeze–thaw cycles through microstructure testing. We took the loess in the Ili landslide in the seasonally frozen region as the research object. Different initial moisture contents and different freeze–thaw cycles were considered as influencing factors for a comparative analysis, of the evolution laws of the stress–strain relationship, failure strength, and shear strength parameters of loess samples. Qualitative and quantitative evaluations were conducted through SEM images to reveal the deterioration mechanism of Ili loess strength under freeze–thaw. Analyzing the evolution of mechanical properties of loess in freeze–thaw environments from both macro and micro perspectives is beneficial for improving the research of loess mechanics theory. More importantly, this work can not only provide important calculation parameters for evaluating the stability of foundation and engineering slopes, ensuring the safe of engineering in cold regions, but also can provide a theoretical basis for future disaster prevention and mitigation in the Ili region, which is of great significance in promoting the construction of the core area of the Silk Road Economic Belt.

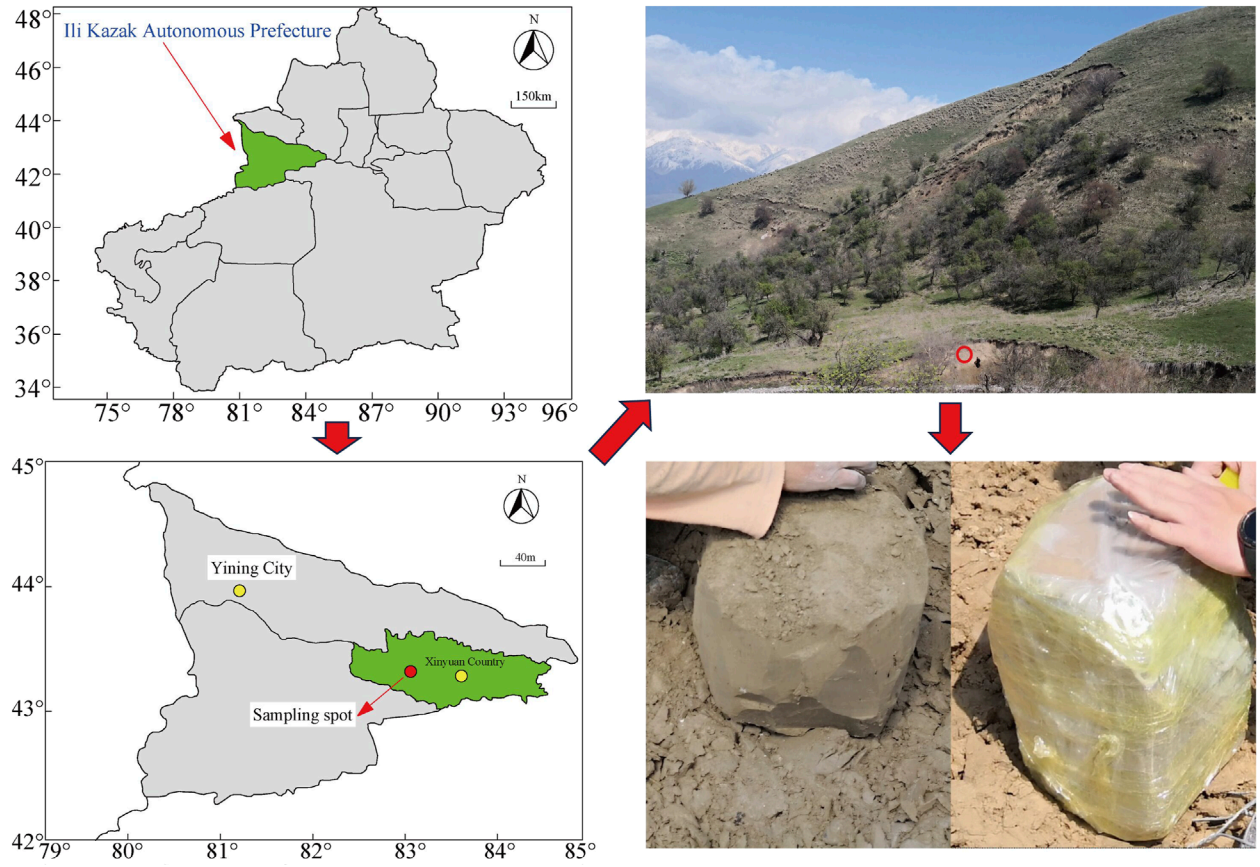

FIGURE 1
Sampling spot at Xinyuan Country.

2 Materials and methods

2.1 Materials

To study the mechanical properties of the Ili loess under freeze–thaw conditions, samples were taken from the Haindesayi Gully loess landslide in Almaler Town, Xinyuan County (as shown in Figure 1), with a sampling depth of 2 m and classified as Q_4 loess. Six sets of undisturbed samples were obtained using a cutting ring to determine the natural density of the loess. Many disturbed soil samples were collected for the physical and mechanical tests.

The physical properties of the Ili loess are listed in Table 1. Through X–ray, mineral composition was determined to be quartz, albite, calcite, lepidolite, and chlorite, with percentages of 21.53, 50.66, 11.22, 12.02, and 4.57, respectively, as shown in Figure 2. Particle size distribution curve obtained by a laser particle size analys is shown in Figure 3, with particles dominated by 20–50 μm and followed by 5–20 μm, contributing a total of 75.2%. According to the soil classification standard, Ili loess is classified as low–liquid–limit clay, with coefficient of nonuniformity (C_u) 18.14 and coefficient of curvature (C_c) 0.50, indicating that uneven, poorly graded particle size, and uneven porosity distribution.

2.2 Sample preparation

Previous studies have shown that freeze–thaw has different effects on soil with different initial moisture contents (Xu et al., 2018; Wang et al., 2010; Ye et al., 2018; Qian, 2018). Remolded samples were used in this experiment to ensure uniformity of each group of samples, First, loose soil samples taken from the field were thoroughly air–dried and their dry moisture content is measured. Five sets of moisture contents were set at 6%, 10%, 14%, 18% and 22% based on the plastic limit of the Ili loess, which are consistent with the dry density of the original soil on site, with a dry density of 1.4 g/cm^3. Masses of dry soil samples and water required for each group were calculated. Distilled water was sprayed multiple times into the soil, and the soil samples were wrapped with preservative film and placed in moisturising container for 48 h to be fully moistened, while controlling the moisture content error to within 1%. Those samples were prepared for triaxial shear and microstructural tests. Next, according to the "Standard for Soil Test Methods GB/T5023–2019," 120 cylindrical samples with a diameter of 39.1 mm and a height of 80 mm were prepared using the tapping method and compacted in 4 layers (Figure 4B). Finally, the samples were wrapped and sealed with plastic film for the freeze–thaw test to avoid water evaporation.

TABLE 1 Basic physical parameters of loess in ili.

Specific gravity (*Gs*)	Natural density (ρ)	Dry density (ρ_d)	Natural water content (w)	Void ratio (e)	Plastic limit (w_p)	Liquid limit (w_L)	Plastic Index (I_p)
2.74	1.70	1.40	18.9%	1.0	21.80%	29.40%	7.60

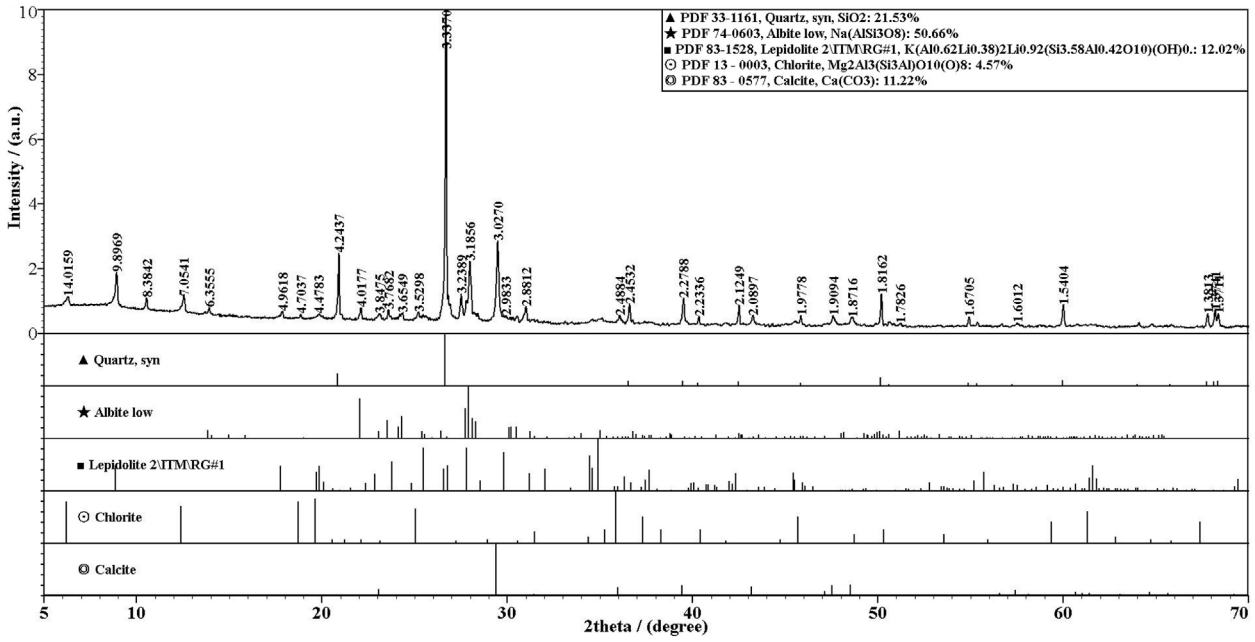

FIGURE 2
The X–ray diffraction patterns of samples.

2.3 Test method

2.3.1 Freeze–thaw test

A programmable high/low–temperature test device with constant temperature and humidity (Figure 4C) was used for the freeze–thaw test in this study. Based on local meteorological data of Xinyuan County, freezing and thawing temperature for this experiment were set at −20°C and 20°C, respectively, and freeze–thaw procedure lasted 16 h (8 h for freezing and 8 h for thawing), completing one freeze–thaw process. According to previous experimental research (Ye et al., 2018; Qian, 2018), after the 15th freeze–thaw cycle, the physical and mechanical properties of the soil mass reached stability. Therefore, the number of freeze–thaw cycles in this experiment was considered as 0, 1, 3, 6, 10, and 20. After the freeze–thaw process, the samples are were removed for subsequent microscopic structure and triaxial shear tests.

2.3.2 Triaxial shear test

To understand the characteristics of the triaxial shear strength and stress–strain relationship curve of the Ili loess after freeze–thaw cycles, TFB–1 unsaturated soil stress–strain triaxial apparatus (Nanjing Soil Instrument Co., Ltd.). (Figure 4D). was used for the triaxial shear test. Considering the influence of consolidation on the mechanical properties of soil, undrained consolidation method was adopted in this experiment, with confining pressure of 50, 100, and 200 kPa, and equal strain rate of 0.1 mm/min. According to the Chinese geotechnical testing method standards, the test was terminated when the axial strain reaches 15%.

2.3.3 Microstructure test

Firstly, after undergoing a specified number of freeze–thaw cycles, the samples were dried naturally. Following this, they were cut into cuboids of 10 × 10 × 20 mm by using a blade, and then the middle section in the height direction was broken to form a fresh section, and the floating soil was blown away with a rubber suction bulb. After that, a gold–sputtering process, which was crucial for obtaining clear and high–quality SEM images, was carried out to enhance the conductivity for electron microscopy. Lastly, the samples were placed on a Quanta 250 FEG SEM (FEI Company; Hillsboro, OR, United States) (Figure 4D). The four corner points and the middle point on the horizontal plane of the cube sample were selected as representative observation points to obtain SEM images at different magnifications, avoiding positions with large holes, impurities, and unevenness.

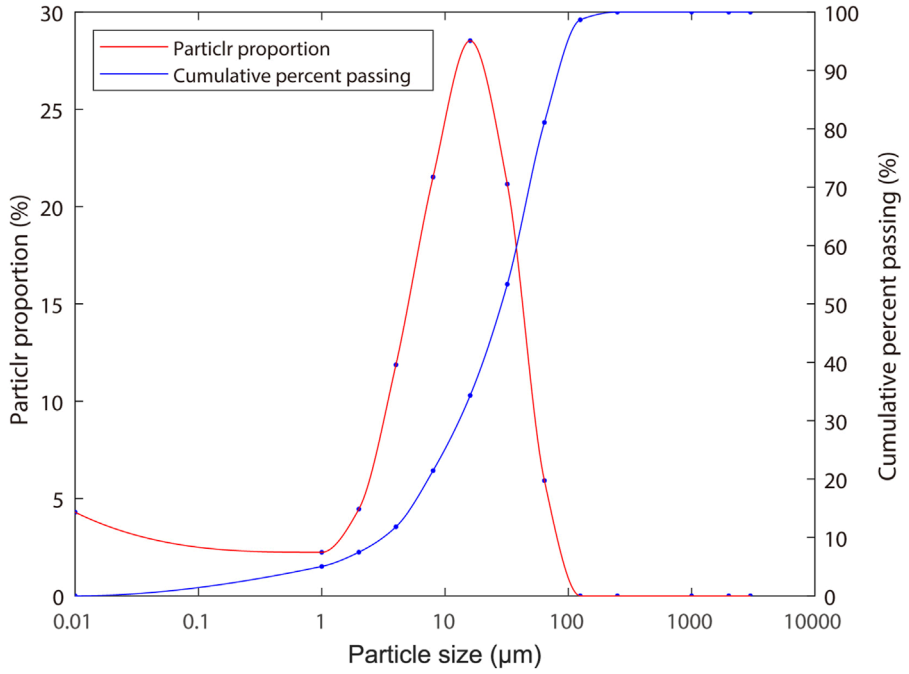

FIGURE 3
Soil particle size distribution curve.

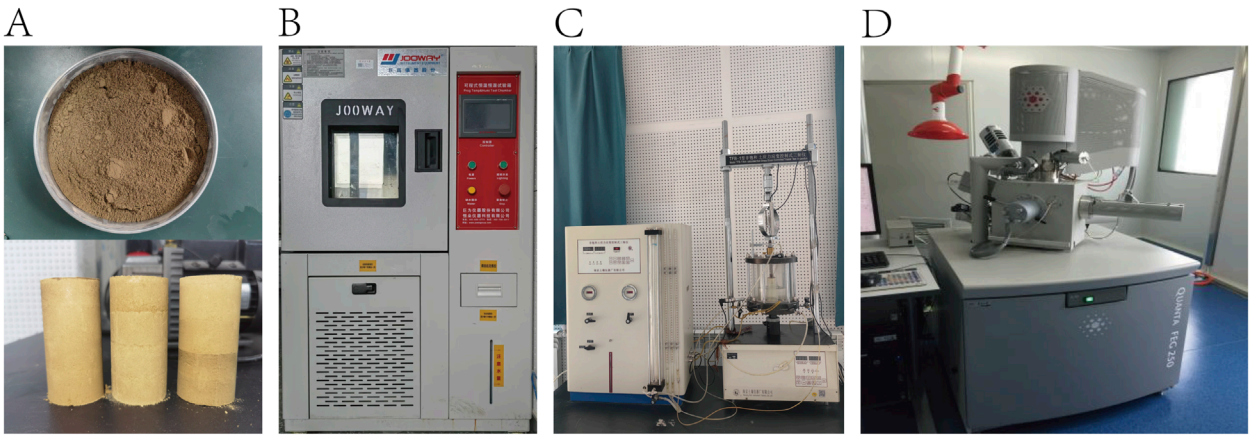

FIGURE 4
Test process: **(A)** Remolded loess, **(B)** High/low–temperature test device used for freeze–thaw test **(C)** Strain–control triaxial instrument, **(D)** The SEM used for Microstructure test.

To explore microscopic mechanism of freeze–thaw effects on loess samples, the microstructure characteristics of loess were analyzed in depth from SEM images. Firstly, the SEM images were qualitatively identified, including particle characteristics and pore characteristics. Then, the computer image processing technology IPP6.0 was used to extract microstructure parameters (including particle size and pore distribution area), and the quantitative analysis of the variation law of loess microstructure with the number of freeze–thaw cycles was carried out.

3 Results and analysis

3.1 Macroscopic characteristics of loess sample under freeze–thaw cycles

3.1.1 Stress–strain curves

Figure 4 shows the stress–strain curves of the loess samples subjected to freeze–thaw cycles. Owing to space limitations, only the results of the loess samples with initial moisture contents of 10% and 18% are presented in this paper. The more the number

of cycles, the lower the corresponding curve position, and with different failure modes of the low and high–water–content curves (Figure 5). For loess samples with an initial moisture content of 10%, under the confining pressure of 50 kPa and 100 kPa, with the increase in freeze–thaw cycles, the peak point of the curve gradually disappears, and the failure mode transitioned from strain softening to strain hardening, with six cycles as the critical value. When the loess samples were subjected to a confining pressure of 200 kPa, peak point was not observed in the stress–strain curves, and the failure mode of the sample was mainly strain hardening, which is consistent with the general law that loess exhibits strain softening behavior under low confining pressure and strain hardening behaviour under high confining pressure (Li et al., 2019). For loess samples with a moisture content of 18%, peak point was not observed in the stress–strain curve, and the type of stress–strain curve changed from strong to weak hardening with increasing cycle number. Figure 6 presents the failure modes of the loess samples with moisture contents of 10% and 18%. Evidently, the loess with moisture content of 10% mainly exhibits brittle failure when the confining pressure was less than or equal to 100 kPa, and plastic failure when the confining pressure reached 200 kPa. Loess samples with a moisture content of 18% exhibited plastic failure, which is consistent with the shape of the curve in Figure 5.

We found that moisture content, cycle number, and confining pressure all have a certain influence on the stress–strain curve and failure mode of loess samples after freeze–thaw cycles. Pan et al. (2023), and Liu et al. (2023) also highlighted that the stress–strain curve is mainly affected by the number of freeze–thaw cycles, initial moisture content of the sample, and confining pressure. Among them, moisture content has the greatest influence on the stress–strain curve and failure mode (Liu et al., 2021), when the deviatoric stress was small, the stress–strain relationship was close to linear in the initial stage.

3.1.2 Failure strength

Figure 5 shows that that the lower the position of the stress–strain curve, the smaller the principal stress difference. To further study the deterioration effect of freeze–thaw cycles on loess, the peak point of the stress–strain curve or the principal stress difference corresponding to a strain of 15% was considered as the failure strength (PRC, 2019). Variation law of loess failure strength with the number of freeze–thaw cycles and moisture content was analyzed. Figures 7A, C shows the relationship between failure strength of loess samples and different moisture contents and the number of freeze–thaw cycles. Under different confining pressures, variation law of the failure strength of loess samples with the number of freeze–thaw cycles was generally the same. Failure strength of loess samples increased with confining pressure. Under the same confining pressure, the maximum amplitude of failure strength deterioration occurred after one cycle. In addition, the deterioration amplitude gradually decreased with increase in cycle number, and even tended to be stabilise. Loess samples with low moisture content (≤14%), reached stability easier, and the curves showed that moisture content increased from top to bottom. Moreover, failure strength of loess samples with moisture content ≥14% decreased significantly, and the maximum deterioration amplitude occurred after one cycle from the moisture content 10%–14%, and the corresponding deterioration amplitude values under confining pressures of 50, 100, and 200 kPa were 134.9, 202.4, and 152.7 kPa, respectively.

Failure strength curves of loess samples with varying moisture content under a confining pressure of 100 kPa are shown in Figure 7D. Under the same confining pressure, failure strength of the loess samples gradually decreased with increasing moisture content, and the trend for every curve was similar, and could be divided into three stages: slow, steep, and steady decline. The steep decline stage indicates, that the maximum decrease in failure strength occurred when the initial moisture content of the samples ranged from 10% to 14%, and the loess amplitude values corresponding to 0, 1, 3, 6, 10, and 20 cycles were 194.9, 202.4, 187.9, 179.6, 169.6, and 168.2 kPa, respectively.

3.1.3 Shear strength parameters

Shear strength parameters of the soil can be easily calculated based on the Mohr–Coulomb strength theory of soil, (Figure 8). Loess samples cohesion gradually decreased with increase in freeze–thaw cycles, and eventually stabilize (Figure 8A). For samples with lower initial moisture content (≤10%), the slope of the curve was larger before the 6th cycle of freeze–thaw, while for samples with higher initial moisture content (≥14%), the slope of the curve was larger before the 3rd cycle. However, sample loss rate between each cycle was mostly 20%–30%. Figure 8B shows the loss of cohesion was greatest when the initial moisture content increased from 10% to 14%. The corresponding loss amplitude values for 0, 1, 3, 6, 10, and 20 cycles were 50.7, 45.0, 31.6, 20.3 kPa, 19.8, and 21.8 kPa, respectively, and the loss amplitude value relatively decreased as the number of freeze–thaw cycles increased, indicating that loeess strength cohesion decreases rapidly from the unfrozen to the frozen–thawed state.

Variation law of the internal friction angle of loess with the number of freeze–thaw cycles and moisture content is shown in Figures 8C, D. The internal friction angle slowly decreased with the increase in the number of freeze–thaw cycles. When the initial moisture content were 6% and 10%, the variation in the internal friction angle of the loess is very small. When the initial moisture content was ≥14%, the internal friction angle of loess decreased with increase in the number of freeze–thaw cycles, but the maximum decrease was 2.8°. Internal friction angle of the loess showed a decreasing trend with an increase in moisture content, and the trend was the same at different cycles. Before the 6th cycle, the maximum reduction amplitude in the internal friction angle occurred between moisture contents of 14% and 18%.

Overall, shear strength parameters of loess samples decreased with increase in freeze–thaw cycles and then tended to stabilise, which is similar to the result obtained by (Zhao et al., 2023) through triaxial undrained tests. The freeze–thaw cycle had the greatest influence on the cohesion of loess, and the influence trend is similar to the failure strength, which is consistent with previous research findings (Song et al., 2008; Dong et al., 2010; Wang et al., 2010; Ni and Shi, 2014; Ye et al., 2018).

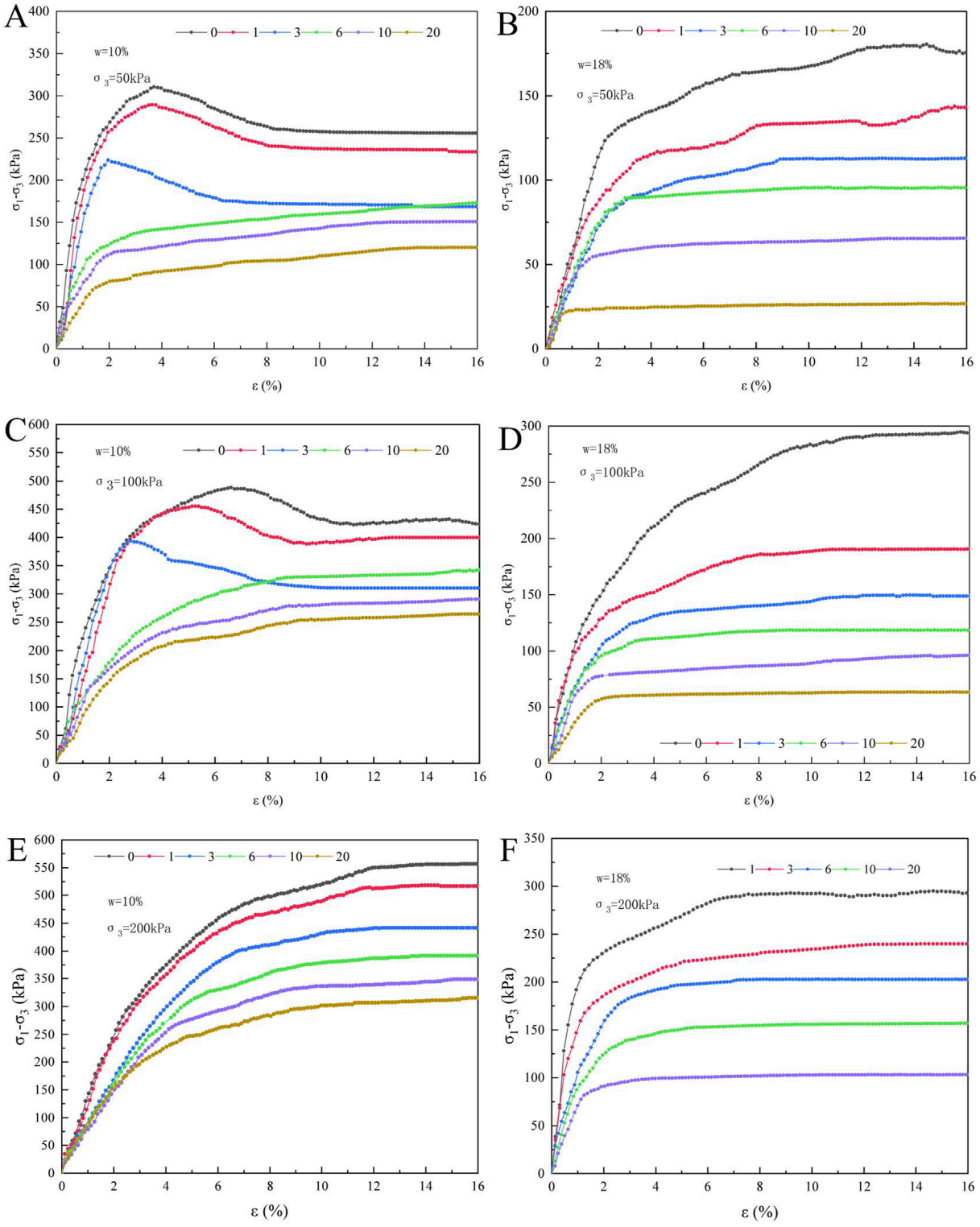

FIGURE 5
Stress–strain curves of samples under freeze–thaw cycles: **(A)** Initial moisture content 10%, confining pressure 50 kPa, **(B)** Initial moisture content 18%, confining pressure 50 kPa, **(C)** Initial moisture content of 10%, confining pressure of 100 kPa, **(D)** Initial moisture content of 18%, confining pressure of 100 kPa, **(E)** Initial moisture content 10%, confining pressure of 200 kPa, **(F)** Initial moisture content of 18%, confining pressure of 200 kPa.

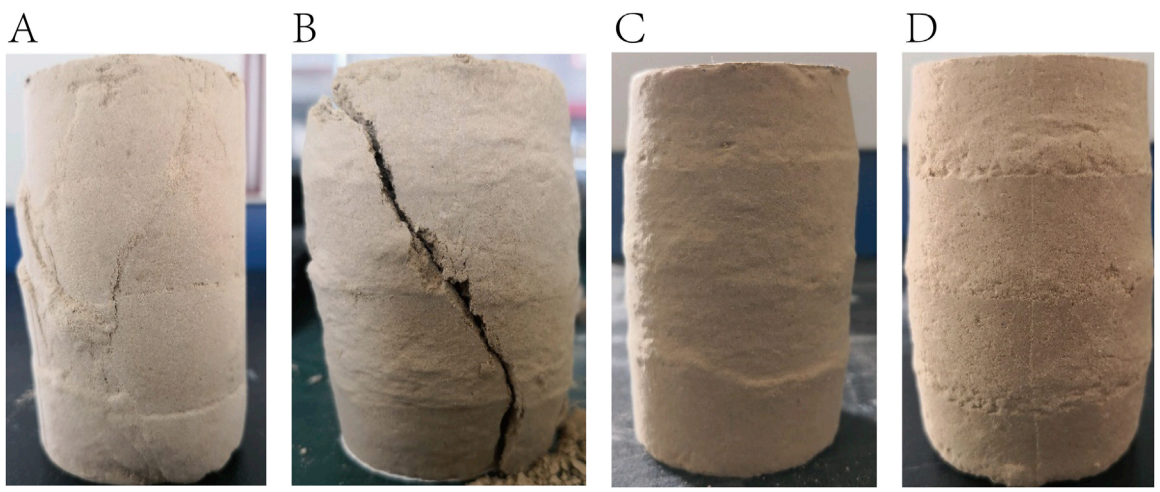

FIGURE 6
Loess samples failure mode under freeze–thaw cycles: **(A)** 10% (100 kPa, 3 times), **(B)** 10% (100 kPa, 6 times), **(C)** 10% (200 kPa, 6 times), **(D)** 18% (200 kPa, 20 times).

3.2 Macroscopic analysis of the loess strength

3.2.1 Fitting of strength parameters

To accurately predict the change law of loess strength subjected to freeze–thaw cycles, further quantitative analysis is required. Therefore, the strength parameters were fitted with the number of freeze–thaw cycles as the independent variable, and the fitting formulas were obtained (Table2). Through fitting, it was found that cohesion is an attenuation exponential function with the number of freeze–thaw cycles as single variable (as shown in Equation 1), which is similar to the power function obtained by Liu et al. in the experiment, but the function expression is different. Furthermore, the change law of the cohesion is a polynomial function (as shown in Equation 2). Fitting parameters A, B, C, D, E, and F for samples with different moisture contents were obtained, and the correlation coefficient R_2 of each fitting equation was almost greater than 0.95, indicating a good fitting degree.

$$y = Ae^{-\frac{x}{B}} + C \tag{1}$$

$$y = D + Ex^2 + Fx \tag{2}$$

where x and y in the formula represent the number of freeze–thaw cycles and strength parameter (cohesion or internal friction angle), which are the independent and dependent variables, respectively.

A sudden change in fitting parameters for cohesion and internal friction angle occurred (Table 2; Figure 9). This can be explained by analysing changes in the fitting parameters. The decrease amplitudes in fitting parameters A and C were 25.228 and 25.828 respectively, with moisture content increasing from 6% to 14%, When the moisture content increased from 14% to 22%, the decrease in fitting parameters A and C was 6.717 and 7.311, respectively. In addition, when moisture content increased from 10% to 14%, parameter D for internal friction angle decreased from 62.445 to 24.511, with a decrease in the amplitude of 37.934. Therefore, moisture content of 14% can be used as the critical moisture content for the variation in the shear strength parameters of the loess. After the moisture content exceeded 14%, parameter D changed slowly, and as the moisture content increased, parameter cohesion B gradually increased, whereas the internal friction angles E and F changed minimally, indicating that changes in moisture content mainly affected parameters A, C, D, and B.

3.2.2 Strength deterioration

To further analyse deterioration degree of triaxial shear strength parameters of loess samples with different moisture contents under freeze–thaw cycles, this study proposes a strength deterioration index L, defined as the degree of strength reduction of loess under freeze–thaw compared to that without freeze–thaw, as shown in Equations 3, 4, to characterise the effect of freeze–thaw cycles on shear strength parameters c and φ of loess.

$$L_c = \frac{c_0 - c_N}{c_0} \times 100\% \tag{3}$$

$$L_\varphi = \frac{\varphi_0 - \varphi_N}{\varphi_0} \times 100\% \tag{4}$$

where L_c and L_φ represent the deterioration of cohesion and internal friction angle, respectively, with the lower subscripts 0 and N representing the number of freeze–thaw cycles of 0 and N, respectively. The value of L is between 0 and 1, with L = 0 indicating no deterioration of the strength indicators, and a higher value of L indicating a higher degree of deterioration.

The deterioration of loess strength parameters was positively correlated with the number of freeze–thaw cycles, and showed an increasing trend with increase in moisture content (Figure 10). The curves of soil samples with moisture content below 14% showed an increasing trend before stabilising, whereas the curves of soil samples with moisture content above 14% showed an increasing trend, but the amplitude of the increase decreased. A comparison deterioration degree of cohesion and internal friction angle revealed that the deterioration degree of cohesion was much greater than that

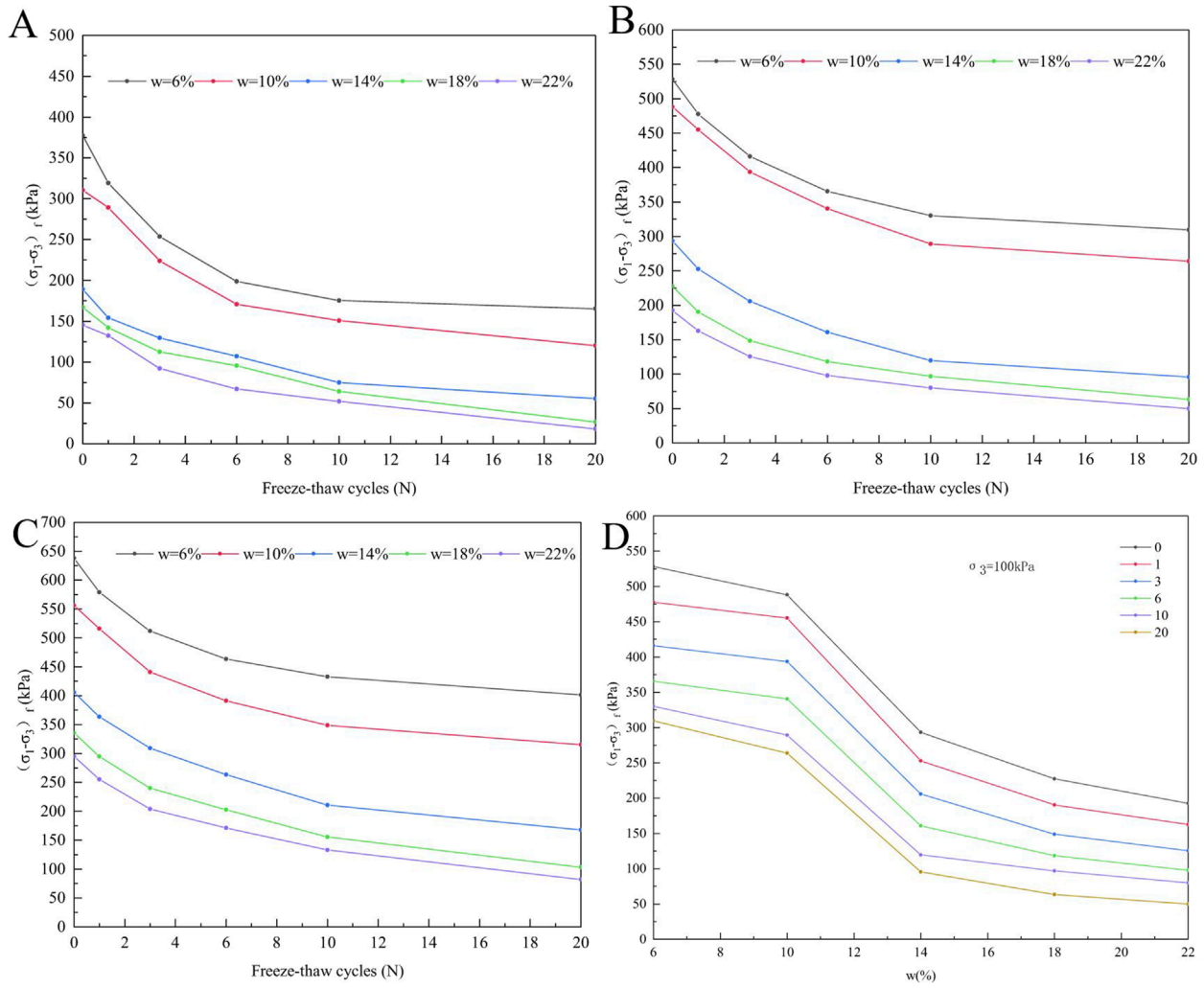

FIGURE 7
Variation law of loess failure strength with the number of freeze–thaw cycles and moisture content: **(A)** Failure strength under confining pressure of 50 kPa, **(B)** Failure strength under confining pressure of 100 kPa, **(C)** Failure strength under confining pressure of 200 kPa, **(D)** Variation of failure strength with moisture content under confining pressure of 100 kPa.

of internal friction angle, which explains why the decrease in the shear strength of loess under a freeze–thaw environment is mainly due to the weakening of cohesion.

3.3 Microscopic characteristics of loess samples under freeze–thaw cycles

3.3.1 Qualitative analysis

Magnifications used for the SEM test were 500, 1,000, 1,500, 2000, and 3,000. After comparison, the ×1,000 magnification image be used to observe overall morphology and complete microstructure (including the shape of particles, contact relationship between particles, particle arrangement, morphology and structure of pores). Although overall morphology was observed at a ×500 magnification, the complete structure could not be distinguished. A higher magnification (over 1,000 magnification) image was exactly the opposite of the lower magnification, therefore, SEM images (magnified 1,000 times) were selected or comparative analysis. Soil samples with initial moisture contents of 10% and 18% were selected, and SEM images (Figure 11) after 0, 3, 6, and 10 freeze–thaw cycles were analysed.

The loess samples without freeze–thaw action (i.e. 0 cycles) contained a relatively high distribution of angular particles, with only a small amount of aggregates in the loess with a moisture content of 18%. Surfaces of the coarse particles were coated with many clay particles, and contact between particles is mostly in the formed of surface–to–surface contact, with a small amount of point–to–surface and point–to–point contact. A large number of medium–sized particles form a mosaic pore structure, whereas some large particles formed an overhead pore structure. As the number of freeze–thaw cycles increased, the number of rounded particles and aggregates begin to increase, and large particles were filled with many small particles. Contact between particles gradually shifted to point–to–point and point–to–surface contacts, and the overhead pore structure gradually became dominant.

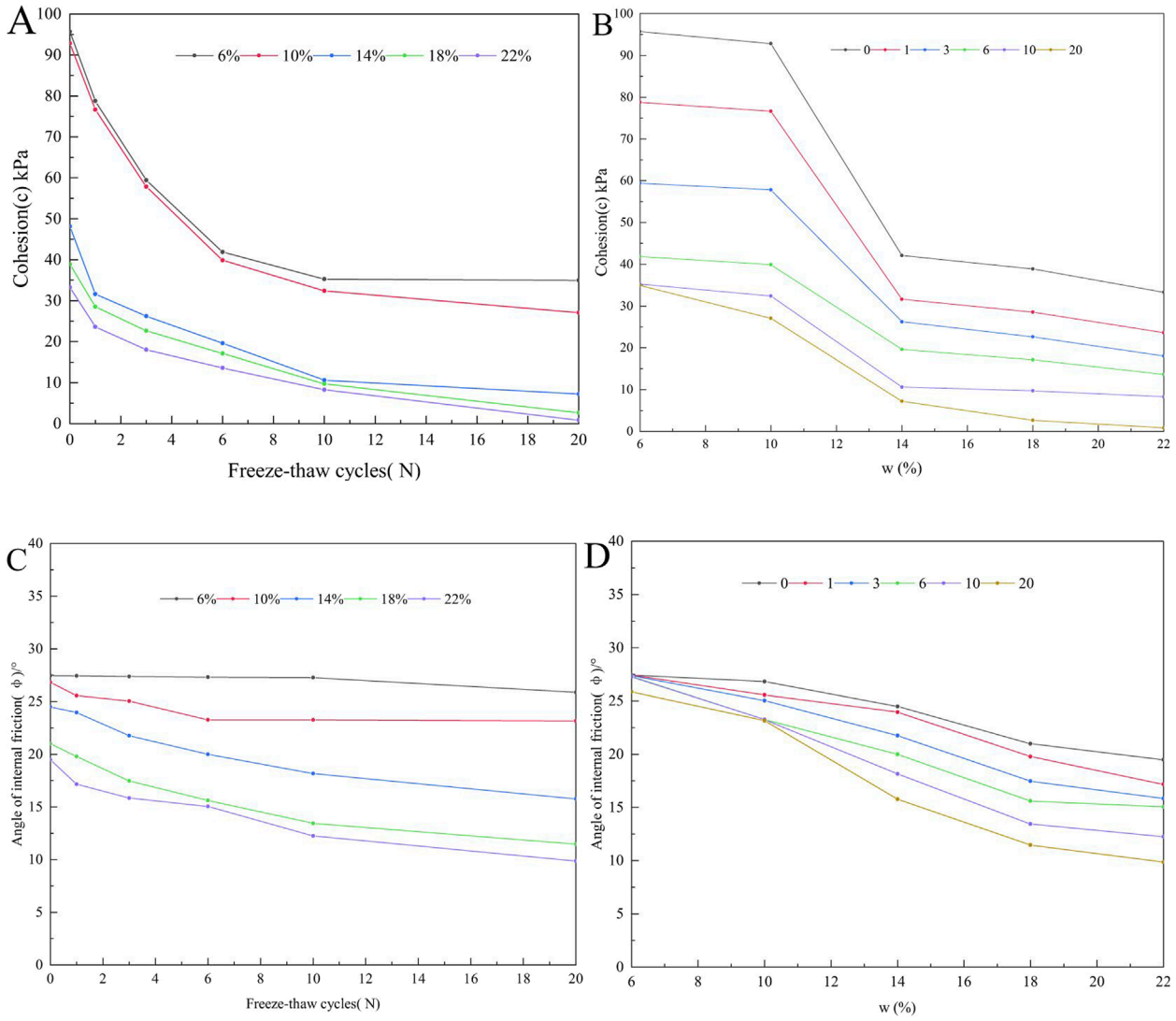

FIGURE 8
Variation of shear strength parameters with the number of freeze–thaw cycles and moisture content: **(A)** The change of cohesion with the number of freeze–thaw cycles, **(B)** The change of cohesion with moisture content, **(C)** The variation of internal friction angle with the number of freeze–thaw cycles, **(D)** Variation of internal friction angle with moisture content.

Evidently, the pore area increased and the particle arrangement was relatively loose. Many small pores were observed inside the aggregates. A comparison of loess samples with initial moisture contents of 10% and 18% revealed that the particles in the samples after 10 freeze–thaw cycles were significantly different, As shown in the SEM images, samples with an initial moisture content of 10% mainly consisted of single detrital grains, with both mosaic and overhead pores, while the particle composition in the soil samples with an initial moisture content of 18% mainly consisted of aggregates with few small particles. The number of freeze–thaw cycles for N = 10 is a critical value, after which the pore area decreases.

3.3.2 Quantitative analysis

According to Gao (2013), loess grain unit is divided into five intervals, d < 2 μm for fine clay particles and colloidal particles, d = 2–5 μm for coarse clay particles, d = 5–10 μm for fine silt particles, d = 10–50 μm for coarse silt particles, d = 50–100 μm for micro–sand particles, and d > 100 μm for sand particles. The particles of remolded loess were mainly <2 μm, followed by 2–5 μm, and the sum of the two could reach about 80%. The distribution of particles >100 μm was the least.

After freeze–thaw cycles, an increasing trend was observed in the content of particles <2 μm in the remolded loess, while a decrease was observed in the content of particles 2–5 μm (Figure 12). A comparion of the remolded loess with initial moisture contents of 10% and 18% revealed that the higher the initial moisture content, the more obvious the trend of increased in the content of particles <2 μm and 10–50 μm with the increase of freeze–thaw cycles, and both exceed the average values under different moisture contents. The percentage content of

TABLE 2 Fitting formula for shear strength parameters.

Parameter	Initial water content (%)	Equation	Correlation Coefficient (R^2)
Cohesion(c) (kPa)	6	$c = 62.226e^{\frac{-N}{3.192}} + 33.601$	0.997
	10	$c = 65.539e^{\frac{-N}{3.843}} + 26.925$	0.999
	14	$c = 36.988e^{\frac{-N}{4.192}} + 7.773$	0.956
	18	$c = 34.738e^{\frac{-N}{6.512}} + 1.696$	0.978
	22	$c = 30.281e^{\frac{-N}{6.432}} + 0.462$	0.998
Angle of internal friction(φ) (°)	6	$\varphi = 27.3905 - 0.0053N^2 + 0.03N$	0.986
	10	$\varphi = 62.445 + 0.021N^2 - 0.0561N$	0.936
	14	$\varphi = 24.5111 + 0.022N^2 - 0.0872N$	0.996
	18	$\varphi = 20.760 + 0.029N^2 - 1.0376N$	0.996
	22	$\varphi = 18.701 + 0.019N^2 - 0.8291N$	0.969

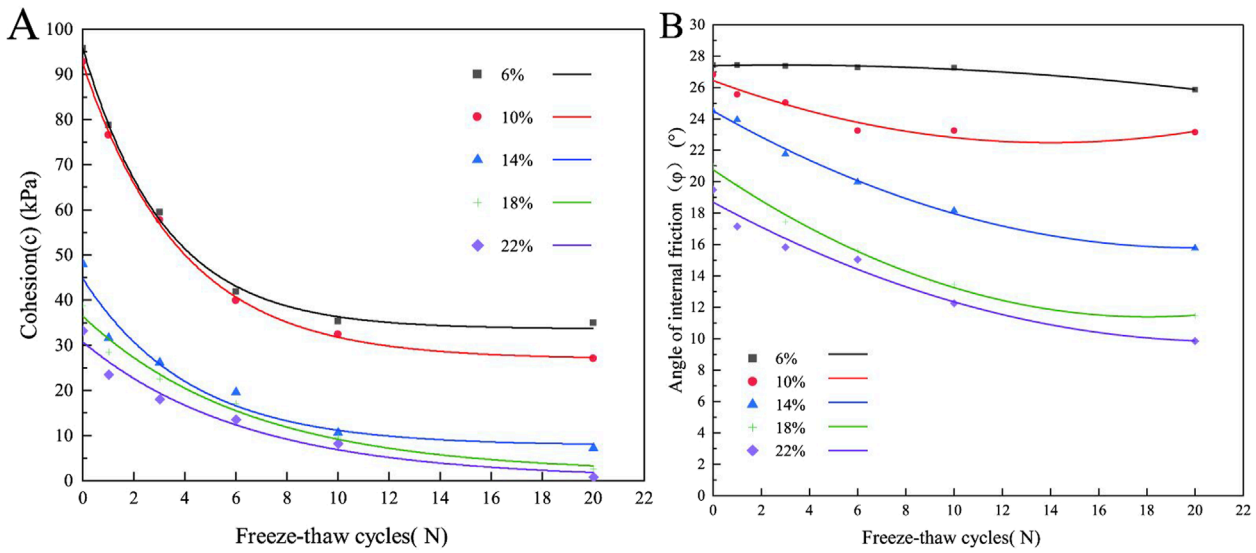

FIGURE 9
Fitting curve of shear strength parameters under freeze–thaw: **(A)** Cohesion, **(B)** Angle of internal friction.

particles <2 μm increases from 55.574% to 69.23%, with a growth percentage of 27.04%, while the trend of decreased in the content of particles 2–5 μm and 5–10 μm became more obvious, and both were lower than the average values under different initial moisture contents.

These findings indicates that the freeze–thaw cycle has a minimal influence on particle distribution of loess with a low moisture content of 10%, and the content of each particle group is relatively concentrated. However, the freeze–thaw cycle had a significant influence on particle distribution of loess with a high moisture content of 18%. It can be concluded that the expansion force of ice crystals formed during freeze–thaw action on loess with high moisture content and the transformation effect on loess particles after thawing are very strong (Xu et al., 2018, Wang et al., 2010).

Figure 13 shows variation in porosity of loess with different initial moisture contents after the freeze–thaw cycles. It can be observed that porosity of loess generally increased first and then decreased with increase in freeze–thaw cycles, reaching a peak. For low moisture content (6% ~ 14%) loess, the peak point occurred at 10 freeze–thaw cycles, whereas for high moisture content (18% ~ 22%) loess, the required number of freeze–thaw cycles for the peak point was relatively small. The freeze–thaw cycle

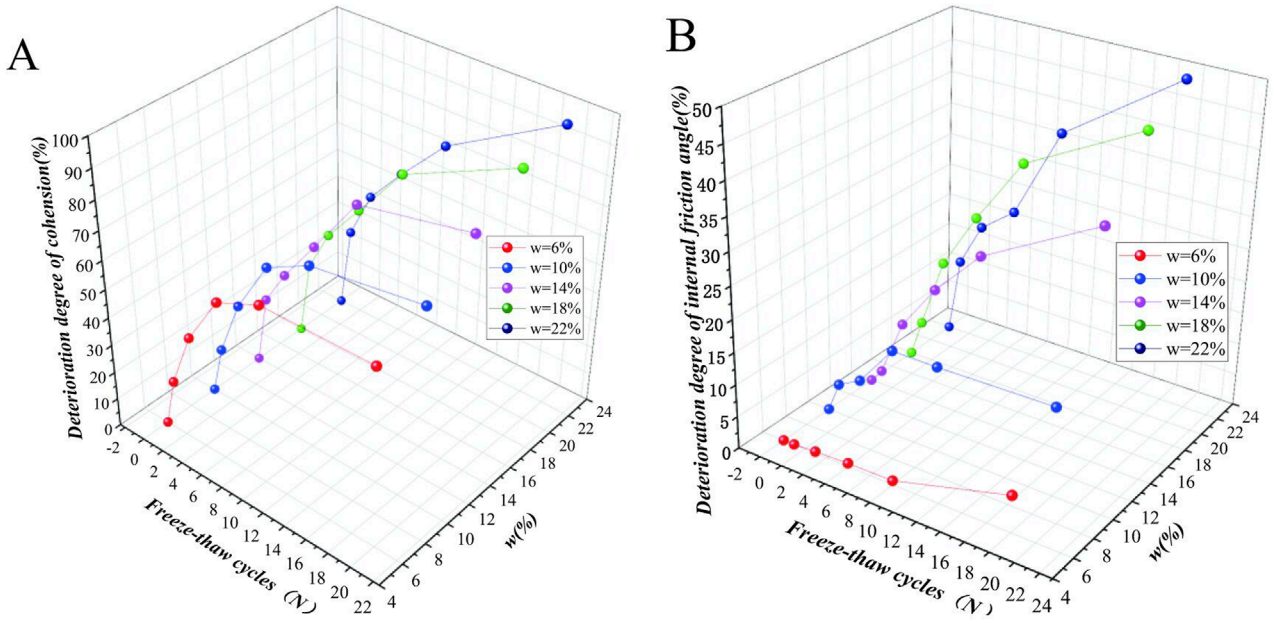

FIGURE 10
Degree of deterioration of loess strength parameters: **(A)** Cohesion, **(B)** Angle of internal friction.

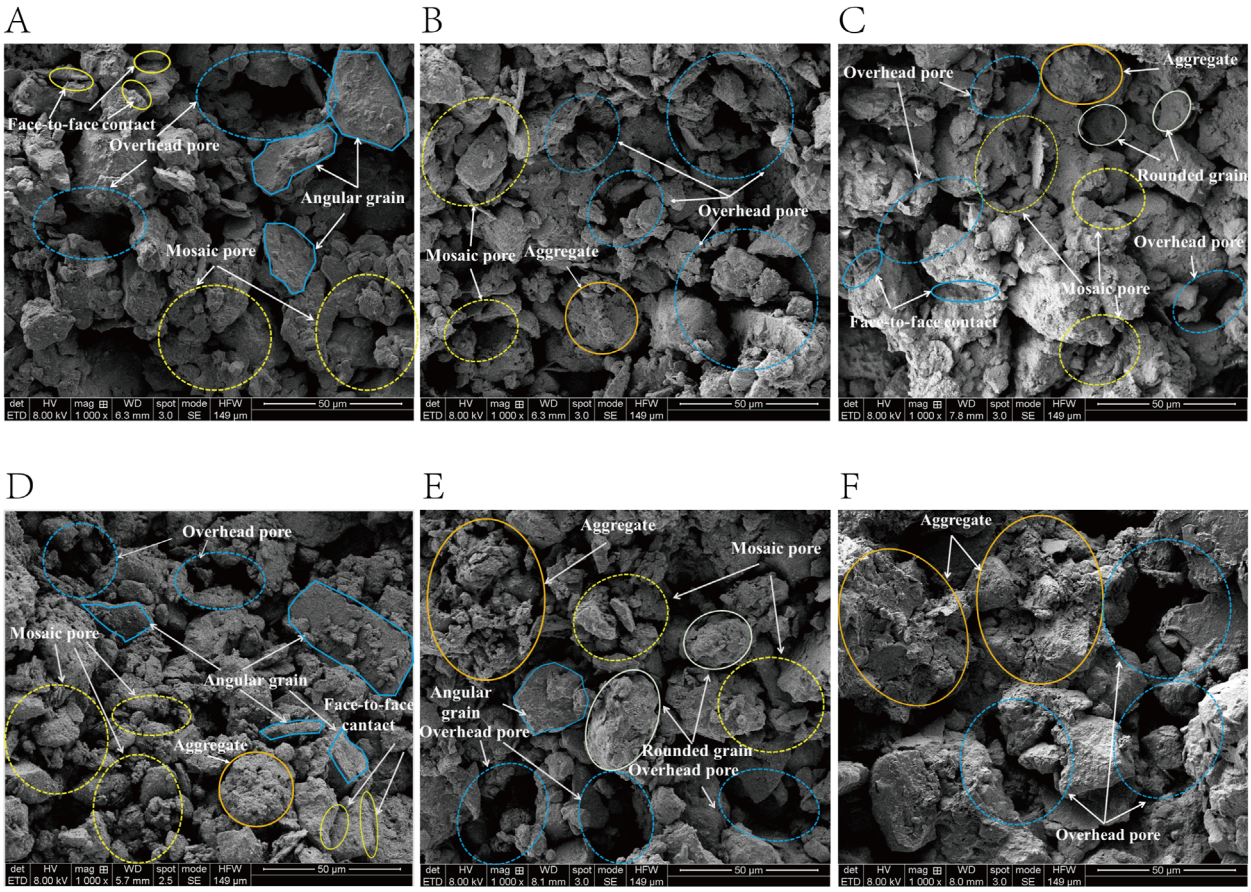

FIGURE 11
SEM images of loess samples after freeze–thaw cycles: **(A)** 10%, 0 time, **(B)** 10%, 6 times, **(C)** 10%,10 times, **(D)** 18%, 0 time, **(E)** 18%, 6 times, **(F)** 18%, 10 times.

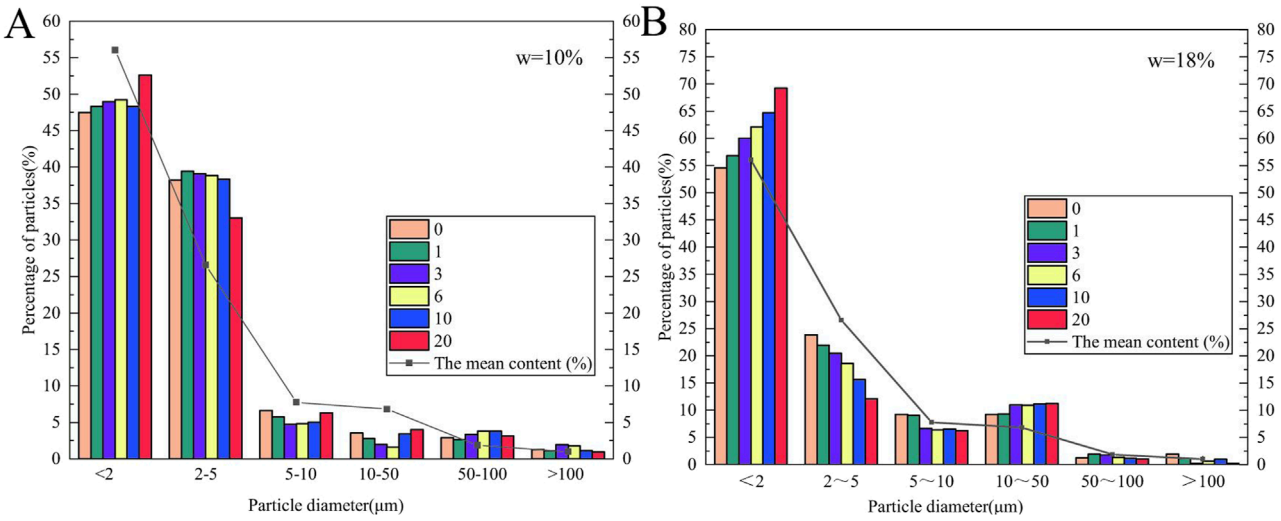

FIGURE 12
Column graph of the percentage content of particle groups after freeze–thaw cycles: **(A)** Initial moisture content 10%, **(B)** Initial moisture content 18%.

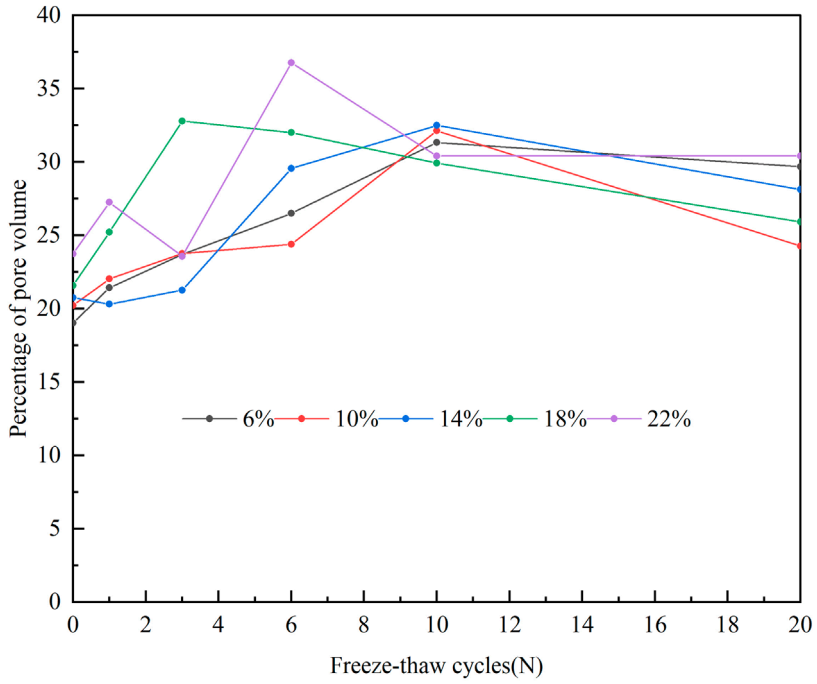

FIGURE 13
Variation curve of porosity after freeze–thaw cycles of loess with different initial moisture contents.

had a significant influence on the porosity of loess with high moisture content, indicating that when the moisture content is high, the frost heaving effect was more pronounced, and the formation of ice crystals caused the loess pores to expand, resulting in the penetration of small pores to form large and medium pores (Mu et al., 2011).

4 Discussion

Loess is a highly water-sensitive and special type of soil. Repeated decrease and increase in temperature in seasonally frozen regions cause changes in the morphology of water in the pores of loess, exhibiting mutual transformation between

liquid and solid phases, and continuous migration of internal water molecules. Ultimately, macroscopic deterioration of loess mechanical properties caused by freeze–thaw cycles is the external manifestation of damage to the internal microstructure.

The microscopic mechanism of loess under freeze–thaw action is illustrated in Figure 14. The loess skeleton is mainly composed of granular units with direct contact between the particles and a small amount of cementation at the contact point. The strength of the contact point p_s (i.e., intergranular pressure, as shown in Figure 14) is mainly composed of the effective stress p_1 transmitted by the overlying load, bonding force p_2 generated by the cementation at the contact point, normal stress p_3 generated by the curved liquid surface between the particles, and the p_4 comprised of the double layer suction and frictional resistance formed by high concentration of dielectric and extremely thin hydration viscous film at the contact point respectively (Gao, 2013). Cohesion value of loess depends on the strength of the contact point between the particles. After freeze–thaw cycles, the structure of loess is damaged owing to the significant extrusion stress caused by the expansion of ice crystals during freezing. As the temperature rises, the soil melts, the arrangement of soil particles becomes loose, and bonding force p_2 between particles decreases (Wang et al., 2010; Li et al., 2018; Ye and Li, 2019; Ye et al., 2020; Liu et al., 2021). From the SEM image as shown in Figure 11, after multiple freeze–thaw cycles, the number of mosaic pores inside the sample decreased and the number of overhead pores increased, resulting in a metastable soil structure. This also indicated that the pore volume of the entire sample increased, which weakened the particle density and cohesion. Therefore, compared with that of the specimens that did not undergo freeze–thaw cycles, the strength of the specimens after freeze–thaw cycles significantly deteriorated, which also indicates that the maximum loss of cohesion occurs in the first cycle (Figure 8). Ye and Li (2019) indicated that irreversible medium and large pores were formed because the large volume of ice crystals exceeded the range of the bonding force of cementation, resulting in a large number of overhead pores. Some scholars have also highlighted reciprocating movement of water causes continuous dissolution of cementation between particles under multiple freeze–thaw cycles, directly weakening the solidification cohesion between structures (Liu et al., 2021; Zhao et al., 2023). However, when the moisture content is high, the bonded water film thickens, extrusion stress formed by ice crystals increases, and structural destruction of the soil intensifies (Xu et al., 2018). Therefore, through experiments, we found that the initial moisture content had a significant influence on the strength parameters of loess in freeze–thaw environments. As the initial moisture content increased, both the cohesion and failure strength decreased. The initial water content of the soil reflects the magnitude of the capillary force (surface) tension p_3 between the particles. The higher the water content, the smaller the capillary force and contact force between the particles, and the lower the cohesion. When the initial moisture content of the sample is high, electrolyte content in the aqueous solution, interparticle attraction p_4 decreases, and bonding force decrease (Li et al., 2018; Gao, 2013).

Owing to the low content of clay particles in loess, insufficient colloids are formed between the soil skeletons, making it a highly dispersed material. The freeze–thaw effect strongly breaks the structure of the soil, not only changing the arrangement, connection, and pore structure of soil particles, but also significantly impacting on the contact mode and shape of the particles. After freeze–thaw cycles, the contact mode between particles gradually changed from face–to–face to point–to–point contact. Compared with those in the face–to–face contact, the connection points between the particles formed by point–to–point contact decreased, resulting in a decrease in the internal friction angle (Zhao et al., 2023). Change in particle shape significantly contribut to the internal friction angle, mainly manifested in the increase in roundness of particles after freeze–thaw, which makes the contact surface smoother and reduces contact points, and interlocking force between particles. The interlocking force between the particles was the strongest when the particles were mainly angular. Compared with that of rounded particles, their movement or rolling needs to overcome a longer path, resulting in a larger internal friction angle. Figure 11 showed that when the number of freeze–thaw cycles was low, the particles were mainly subangular, and as the number of freeze–thaw cycles increases, they are mainly rounded. Therefore, the freeze–thaw effect weakens the friction angle of the loess.

The above analyses indicate that the deterioration mechanism of loess strength parameters under freeze–thaw action is complex and influenced by multiple factors. Both the moisture content and dry density have a significant impact on loess cohesion (Xu et al., 2018). Expansion force generated by ice crystal formation can cause the formation of cracks within the soil during the low–temperature freezing process. In addition, original loess is characterized as the distribution of discontinuous surfaces with various origins and morphologies. Therefore, focusing on analysis of crack initiation under various factor is also crucial for understanding the evolution of mechanical properties and the failure mode (Bi et al., 2016; Zhou et al., 2019; Zhao et al., 2020; Zhao et al., 2021; Zhao et al., 2023). However, no obvious cracks were observed in the SEM images of this study, which may be related to the fact that loess samples in this study were remolded with a low dry density, and ware relatively loose. The influence of crack initiation on the mechanical properties of loess in freeze–thaw environments should also be considered in future study. Moreover, attention should be paid to the original samples to better study the mechanical evolution of Ili loess under freeze–thaw conditions from the analyzing crack initiation perspectives.

Loess landslides are widely distributed in the Ili region, and previous studies have shown that their formation mechanism is closely related to seasonal freeze–thaw effects. Freezing and thawing, as strong weathering effects in seasonally frozen regions, break the soil structure, and frost heave effect intensifies the expansion of cracks in loess slopes, providing a good seepage channel for snow melt and rainfall infiltration. Under this repeated freeze–thaw action, mechanical properties of the surface soil substantially deteriorated, promoting the occurrence of landslides. With the promotion of 'the Belt and Road', various engineering constructions have increased, and landslide hazards in the Ili area have intensified. To reduce the harm caused by such disasters, improving the monitoring technology for landslide disasters and monitoring key landslides and regional disasters is necessary. Currently, high–precision global navigation satellite system technology (Nikolakopoulos et al., 2023; Wang et al., 2023; Huang et al., 2023) is being used globally. Through this technology, an automatic deformation monitoring system has been established, and data on rainfall, snowfall, temperature, moisture content,

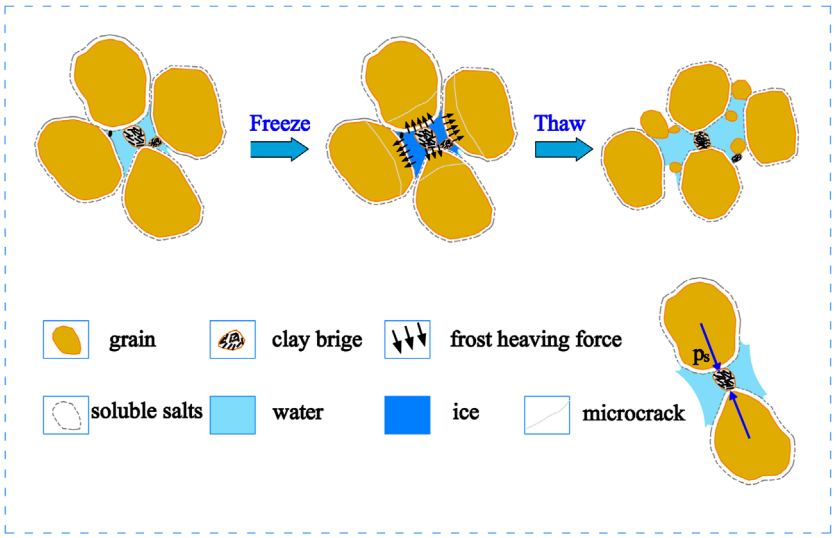

FIGURE 14
Schematic diagram of microstructure evolution of loess under freeze–thaw action.

surface deformation, and cracks are obtained based on the characteristics of landslide mechanisms in the Ili region, establishing early–warning models and combineing 3D image recognition technology to achieve dynamic monitoring of geological hazards (Gu et al., 2023; Li et al., 2023).

5 Conclusion

To study the characteristics and deterioration mechanism of freeze–thaw action on the shear strength of Ili loess, indoor triaxial shear tests and microstructural tests were conducted on 30 sets of loess samples with different freeze–thaw cycles and moisture contents. The following conclusions were drawn:

(1) With the increase in the number of freeze–thaw cycles, the failure mode of the stress–strain curve of low–moisture loess samples (≤10%) changes from strain softening to strain hardening, with the critical point 6 freeze–thaw cycles. Failure mode of the stress-strain curve follows a similar pattern with the increase of confining pressure. However, for loess samples with moisture content of 18%, as the number of cycles increased, the stress–strain curve changed from strong softening to weak hardening.

(2) Freeze–thaw cycle have a significant weakening effect on the failure and shear strength parameters of loess. The curve of the failure strength with the number of freeze–thaw cycles presents three stages of development: slow, steep decline, and steady decline, and the trend of decreasing cohesion values is similar to that of the strength of failure. Simultaneously, comparison of the shear strength parameters of loess revealed that freeze–thaw action has the greatest effect on the cohesion of loess. The degradation is strong after the first freeze–thaw cycle. In addition, after the 10th cycle, the weakening effect gradually slowed down. However, the internal friction angle decreased slowly with an increase in number of freeze–thaw cycles. The initial moisture content also has a significant influence on cohesion, manifested as a significant deterioration of cohesion with fewer freeze–thaw cycles when moisture content is high. Similar patterns were observed on degree of deterioration.

(3) By fitting, it was found that the cohesion and internal friction angle exhibit an attenuation exponential function and a polynomial function relationship with the number of freeze–thaw cycles, respectively. The main fitting parameters showed a sudden change with an increase in moisture content, with a turning point of 14%. This function provides a theoretical basis for disaster prevention and mitigation of loess landslides.

(4) Qualitative and quantitative analysis of SEM images indicate that the content of particle groups changes significantly with the number of freeze–thaw cycles; with an increase in freeze–thaw cycles, the number of overhead pores increases and number of mosaic pores decreases, contact mode of particles changes from point–to–plane to point–to–point. Overall, the porosity of loess shows a an increasing trend first and then decreasing with an increase in freeze–thaw cycles, the freeze–thaw cycle has a strong influence on the porosity of loess with high moisture content, indicating that freeze–thaw has a stronger effect on transformation of loess particles when moisture content is high. The above microstructural changes fully explain the deterioration of the shear strength parameters of the loess samples under freeze–thaw action.

(5) Analyses of the changes in the microstructure after freeze–thaw action, which led to a decrease in the strength p_s between the contact points and an increase in moisture content weakening p_s, demonstrated the deterioration of the shear strength parameters of loess samples under freeze–thaw action. Furthermore, the degradation

mechanism of the microstructure under freeze–thaw action was revealed.

(6) In this study, soil samples were remolded, which can ensure uniformity of each group of samples. However, structures of the remolded samples were not identical to those of the original samples. To better understand the degradation of the freeze–thaw effect on original samples, analyzing crack initiation is necessary to strengthen research on the samples and test their mechanical degradation evolution under freeze–thaw conditions in the future.

Data availability statement

The original contributions presented in the study are included in the article/supplementary material, further inquiries can be directed to the corresponding authors.

Author contributions

CC: Data curation, Formal Analysis, Funding acquisition, Investigation, Methodology, Supervision, Writing–original draft, Writing–review and editing. LY: Formal Analysis, Investigation, Supervision, Writing–review and editing. WC: Data curation, Formal Analysis, Methodology, Writing–review and editing. JW: Formal Analysis, Software, Writing–original draft. XW: Software, Writing–original draft.

Funding

The author(s) declare that financial support was received for the research, authorship, and/or publication of this article. This research was funded by Natural Science Foundation of Xinjiang Uygur Autonomous Region (2021D01C043) and the Undergraduate Training Program for Innovation of Xinjiang Uygur Autonomous Region (S202310755009).

Acknowledgments

The authors gratefully acknowledge the financial support from the Natural Science Foundation of Xinjiang Uygur Autonomous Region and Undergraduate Training Program for Innovation of Xinjiang Uygur Autonomous Region.

Conflict of interest

Author LY was employed by Wuhan Design & Research Institute Co., Ltd. of China Coal Technology and Engineering Group.

The remaining authors declare that the research was conducted in the absence of any commercial or financial relationships that could be construed as a potential conflict of interest.

Publisher's note

All claims expressed in this article are solely those of the authors and do not necessarily represent those of their affiliated organizations, or those of the publisher, the editors and the reviewers. Any product that may be evaluated in this article, or claim that may be made by its manufacturer, is not guaranteed or endorsed by the publisher.

References

An, P., Zhang, A. J., Xing, Y. C., Ni, W., and Ren, W. (2018). Experimental study on settling characteristics of thick self–weight collapsible loess in Xinjiang Ili region in China using field immersion test. *Soils Found.* 58 (6), 1476–1491. doi:10.1016/j.sandf.2018.08.005

Bi, J., Zhou, X. P., and Qian, Q. H. (2016). The 3D numerical simulation for the propagation process of multiple pre–existing flaws in rock–like materials subjected to biaxial compressive loads. *Rock Mech. Rock Eng.* 49 (5), 1611–1627. doi:10.1007/s00603–015–0867–y

Bragar, E., Pronozin, Y., Zhussupbekov, A., Sarsembayeva, A., Muzdybayeva, T., et al. (2022). Evaluation of the strength characteristics of silty-clayey soils during freezing-thawing cycles. *Appl. Sci.* 12, 802. doi:10.3390/app12020802

Dong, X. H., Zhang, A. J., and Lian, J. B. (2010). Laboratory study on shear strength deterioration of loess with long–term freezing–thawing cycles. *J. Eng. Geol.* 18, 1004–9665.

Gao, G. (2013). *Neoteric soil geotechnology* (second edition). Science Press: Beijing.

Gu, X., Nie, W., Geng, J., Zhu, T., and Zheng, S. (2023). Road slope monitoring and early warning system integrating numerical simulation and image recognition: a case study of Nanping, Fujian, China. *Stoch. Environ. Res. Risk Assess.* 37 (10), 3819–3835. doi:10.1007/s00477–023–02482–5

Hong, B. N., and Liu, X. (2010). *Theory and experiment of soil microstructures*. Science Press: Beijing.

Hu, W., Cheng, W., and Wang, L. (2022). Micro–structural characteristics deterioration of intact loess under acid and saline solutions and resultant macro–mechanical properties. *Soil Tillage Res.* 220, 105382. doi:10.1016/j.still.2022.105382

Hu, W., Cheng, W., and Wen, S. (2021). Effects of chemical contamination on microscale structural characteristics of intact loess and resultant macroscale mechanical properties. *CATENA* 203, 105361. doi:10.1016/j.catena.2021.105361

Huang, G. D. S. W., Du, S., and Wang, D. (2023). GNSS techniques for real–time monitoring of landslides: a review. *Satell. Navig.* 4, 5. doi:10.1186/s43020–023–00095–5

Ismeik, M., and Shaqour, F. (2020). Effectiveness of lime in stabilising subgrade soils subjected to freeze–thaw cycles. *Road. Mater Pavement* 21, 42–60. doi:10.1080/14680629.2018.1479289

Jing, J. J., Wu, Z. J., Yan, W. J., Liang, C., and Lu, Y. (2022). Experimental study on progressive deformation and failure mode of loess fill slopes under freeze-thaw cycles and earthquakes. *Eng. Geol.* 310, 106896. doi:10.1016/j.enggeo.2022.106896

Kong, J. X., Zhuang, J. Q., Peng, J. B., Zhan, J., and Mu, J. (2023). Failure mechanism and movement process of three loess landslides due to freeze–thaw cycle in the Fangtai village, Yongjing County, Chinese Loess Plateau. *Eng. Geol.* 315, 107030. doi:10.1016/j.enggeo.2023.107030

Li, G. Y., Wang, F., Ma, W., eta, l., Mu, Y., and Mao, Y., (2018). Variations in strength and deformation of compacted loess exposed to wetting–drying and freeze–thaw cycles. *Cold Reg. Sci. Technol.* 151, 159–167. doi:10.1016/j.coldregions.2018.03.021

Li, S., Li, Y., and Gao, X. (2019). Experimental study on the triaxial stress-strain curve of undisturbed loess in xining by freeze-thaw cycles. *Iop Conf. Ser. Earth Environ. Sci.* 304, 052065. doi:10.1088/1755–1315/304/5/052065

Li, Z. Y., Yang, G. S., and Liu, H. (2020). The influence of regional freeze–thaw cycles on loess landslides: analysis of strength deterioration of loess with changes in pore structure. *Water* 12, 3047. doi:10.3390/w12113047

Li, Y., Nie, W., Li, Q., eta, l., Yuan, C., Dai, B., et al. (2023). Prediction of landslide deformation region based on the improved S–growth curve model. *Appl. Sci.* 13, 3555. doi:10.3390/app13063555

Liang, Z., Zhang, A., Ren, W., Hu, H., and Wang, Y. (2023). Investigating the curing time effect on water retention property and microstructure of lime–treated Ili loess. *B Eng. Geol. Environ.* 82, 241. doi:10.1007/s10064–023–03267–4

Liu, K., Ye, W. J., and Jing, H. J. (2021). Shear strength and microstructure of intact loess subjected to freeze–thaw cycling. *Adv. Mater Sci. Eng.* 2021, 1–15. doi:10.1155/2021/1173603

Liu, L. Q., Zhang, W. Y., and Zhang, B. Y. (2021). Effect of freezing–thawing cycles on mechanical properties and microscopic mechanisms of loess. *Hydrogeology Eng. Geol.* 48, 109–115. doi:10.16030/j.cnki.issn.1000-3665.202009064

Liu, Y., Han, D. D., and Liu, N. N. (2023a). Reinforcement mechanism analysis of lattice beam and prestressed anchor rod system for loess slope. *Front. Earth Sci–Prc* 11. doi:10.3389/feart.2023.1121172

Liu, Y. N., Fabbri, A., Wong, H. K. K., Traore, L. B., Li, X., and Pardoen, B. (2023b). Experimental study on the freezing-thawing behavior of compacted earth. *Constr. Build. Mater* 404, 133130. doi:10.1016/j.conbuildmat.2023.133130

Mu, Y. H., Ma, W., and Li, G. Y. (2011). Quantitative analysis of impacts of freeze–thaw cycles upon microstructure of compacted loess. *Chin. J. Geotechnical Eng.* 33, 1919–1925. doi:10.16030/j.cnki

Nguyen, T. T. H., Cui, Y., Ferber, V., Ozturk, T., and Plier, F. (2019). Effect of freeze–thaw cycles on mechanical strength of lime–treated fine–grained soils. *Transp. Geotech.* 21, 100281. doi:10.1016/j.trgeo.2019.100281

Ni, W. K., and Shi, H. Q. (2014). Influence of freezing–thawing cycles on micro–structure and shear strength of loess. *J. Glaciol. Geocryol.* 36, 922–927.

Nie, W., Li, C. X., Hu, J. W., Wang, W., and Luo, M. (2023). Spatial variation of physical and mechanical properties of tailings under different rainfall intensities and the interaction pattern. *Geomechanics Geophys. Geo–Energy Geo–Resources* 9 (1), 86. doi:10.1007/s40948–023–00625–0

Nikolakopoulos, K. G., Kyriou, A., Koukouvelas, I. K., and Lyros, E. (2023). UAV, GNSS, and InSAR data analyses for landslide monitoring in a mountainous village in western Greece. *Remote Sens.* 15, 2870. doi:10.3390/rs15112870

Niu, L. S., Ren, W. Y., Zhang, A. J., Liang, Z., and Han, J. (2021). Experimental study on the influence of soluble salt content on unsaturated mechanical characteristics of undisturbed Ili loess. *Bull. Eng. Geol. Environ.* 80, 6689–6704. doi:10.1007/s10064–021–02340–0

Pan, Z. X., Yang, G. S., Ye, W. J., Liang, B., and Yang, Q. (2023). Effect of freeze–thaw cycles and initial water content on the pore structure and mechanical properties of loess in northern shaanxi. *Sustain. Basel, Switz.* 15, 10937. doi:10.3390/su151410937

Prc, M. O. H. A. (2019). Standard for geotechnical testing method. in *GB/T 50123–2019*, M. O. H. A. PRC,ed. China Planning Press: Beijing.

Qian, C. (2018). *Study on the mechanical properties and structure changes in microscale and mesoscale of loess in Heifangtai under freeze–thaw action*. China University of Geosciences (Beijing), Beijing.

Ren, J., and Vanapalli, S. K. (2020). Effect of freeze–thaw cycling on the soil–freezing characteristic curve of five Canadian soils. *Vadose Zone J.* 19, e20039. doi:10.1002/vzj2.20039

Song, C. X., Qi, J. L., and Liu, F. Y. (2008). Influence of freeze–thaw on mechanical properties of Lanzhou loess. *Rock Soil Mech.* 29, 1077–1080. doi:10.16285/j.rsm.2008.04.048

Wang, D. H. G. D., Huang, G., Du, Y., Zhang, Q., Bai, Z., and Tian, J. (2023). Stability analysis of reference station and compensation for monitoring stations in GNSS landslide monitoring. *Satell. Navig.* 4, 29. doi:10.1186/s43020–023–00119–0

Wang, L. Q., Wang, L., Zhang, W. G., Liu, S., and Zhu, C. (2024). Time series prediction of reservoir bank landslide failure probability considering the spatial variability of soil properties. *J. Rock Mech. Geotechnical Eng.* doi:10.1016/j.jrmge.2023.11.040

Wang, M., Meng, S., Sun, Y., and Fu, H. (2018). Shear strength of frozen clay under freezing-thawing cycles using triaxial tests. *Earthq. Eng. Eng. Vib.* 17, 761–769. doi:10.1007/s11803–018–0474–5

Wang, N. Q., and Yao, Y. (2003). Characteristics and mechanism of landslides in loess during freezing and thawing periods in seasonally frozen ground regions. *J. Disaster Prev. Mitig. Eng.* 28, 163–166.

Wang, S. L., Lv, Q. F., Baaj, H., and Zhao, Y. x. (2016). Volume change behaviour and microstructure of stabilized loess under cyclic freeze–thaw conditions. *Can. J. Civ. Eng.* 43, 865–874. doi:10.1139/cjce–2016–0052

Wang, T. X., Luo, S. F., and Liu, X. J. (2010). Testing study of freezing–thawing strength of unsaturated undisturbed loess considering influence of moisture content. *Rock Soil Mech.* 31, 2378–2382. doi:10.16285/j.rsm.2010.08.044

Wang, Y. G., Zhang, A. J., and Ren, W. Y. (2019). Study on the soil water characteristic curve and its fitting model of Ili loess with high level of soluble salts. *J. Hydrology* 578, 124067. doi:10.1016/j.jhydrol.2019.124067

Wei, C., and Li, G. Y. (2019). Study on the mesostructural evolution mechanism of compacted loess subjected to various weathering actions. *Cold Reg. Sci. Technol.* 167, 102846. doi:10.1016/j.coldregions.2019.102846

Xu, J., Ren, J. W., Wang, Z. Q., and Yuan, J. (2018). Strength behaviors and meso–structural characters of loess after freeze–thaw. *Cold Reg. Sci. Technol.* 148, 104–120. doi:10.1016/j.coldregions.2018.01.011

Xu, J., Wang, Z. Q., and Ren, J. W. (2018). Comparative test study on deterioration mechanism of undisturbed and remolded loess during the freeze–thaw process. *Chin. J. Undergr. Space Eng.* 14, 643–649.

Ye, W. J., Chen, Y., and Zhang, D. (2020). Macro and micro experimental study on the influence of moisture migration on the strength of compacted loess under freeze–thaw. *China J. Highw. Transp.* 2020. doi:10.19721/j.cnki.1001-7372.2021

Ye, W. J., and Li, C. Q. (2019). The consequences of changes in the structure of loess as a result of cyclic freezing and thawing. *B Eng. Geol. Environ.* 78, 2125–2138. doi:10.1007/s10064–018–1252–3

Ye, W. J., Li, C. Q., and Dong, X. H. (2018). Study on damage identification of loess microstructure and macro mechanical response under freezing and thawing conditions. *J. Glaciol. Geocryol.* 40, 546–555. doi:10.7522/j.issn.1000-0240.2018.0059

Yin, Y. P., Wang, L. Q., Zhang, W. G., and Dai, Z. (2022). Research on the collapse process of a thick–layer dangerous rock on the reservoir bank. *Bull. Eng. Geol. Environ.* 81 (3), 109. doi:10.1007/s10064–022–02618–x

Yu, X., Wei, X. L., Zhou, H. B., Liu, Y., Liu, F., et al. (2022). Snowmelt–triggered reactivation of a loess landslide in Yili, Xinjiang, China: mode and mechanism. *Landslides* 19 (8), 1843–1860. doi:10.1007/s10346–022–01879–7

Zhang, J. W., Mu, Q. Y., Garg, A., and Cao, J. (2020). Shear behavior of unsaturated intact and compacted loess: a comparison study. *Environ. Earth Sci.* 79, 79. doi:10.1007/s12665–020–8820–0

Zhang, K. Q., Wang, L. Q., Dai, Z. W., and Zhang, Z. (2022). Evolution trend of the Huangyanwo rock mass under the action of reservoir water fluctuation. *Nat. Hazards* 113, 1583–1600. doi:10.1007/s11069–022–05359–y

Zhang, W. G., Lin, S. C., Wang, L. Q., and Jiang, X. (2024). A novel creep contact model for rock and its implement in discrete element simulation. *Comput. Geotechnics* 167, 106054. doi:10.1016/j.compgeo.2023.106054

Zhao, L., Peng, J., Ma, P., and Ma, Z. (2023). Microstructure response to shear strength deterioration in loess after freeze–thaw cycles. *Eng. Geol.* 323, 107229. doi:10.1016/j.enggeo.2023.107229

Zhao, L. Q., Peng, J. b., and Ma, P. H. (2023). Preliminary research on loess mesoscopic interface and its hazard effect. *J. Eng. Geol.* 31 (6), 1783–1798. doi:10.13544/j.cnki.jeg.2021-0714

Zhao, Y., Bi, J., Wang, C., and Liu, P. (2021). Effect of unloading rate on the mechanical behavior and fracture characteristics of sandstones under complex triaxial stress conditions. *Rock Mech. Rock Eng.* 54 (9), 4851–4866. doi:10.1007/s00603–021–02515–x

Zhao, Y., Wang, C. L., and Bi, J. (2020). Analysis of fractured rock permeability evolution under unloading conditions by the model of elastoplastic contact between rough surfaces. *Rock Mech. Rock Eng.* 53 (12), 5795–5808. doi:10.1007/s00603–020–02224–x

Zheng, P. L., Wang, J. G., Wu, Z. H., and Liu, Q. (2022). Effect of water content variation on the tensile characteristic of clayey loess in Ili Valley, China. *Appl. Sci.* 12 (17), 8470. doi:10.3390/app12178470

Zhou, C., Hu, Y. J., Xiao, T., and Wang, L. (2023). Analytical model for reinforcement effect and load transfer of pre–stressed anchor cable with bore deviation. *Constr. Build. Material* 379, 131219. doi:10.1016/j.conbuildmat.2023.131219

Zhou, X., Wang, Y., Zhang, J., and Liu, F. (2019). Fracturing behavior study of three–flawed specimens by uniaxial compression and 3D digital image correlation: sensitivity to brittleness. *Rock Mech. Rock Eng.* 52 (3), 691–718. doi:10.1007/s00603–018–1600–4

Zhou, Z., Ma, W., Zhang, S., and Li, G. (2018). Effect of freeze–thaw cycles in mechanical behaviors of frozen loess. *Cold Reg. Sci. Technol.* 146, 9–18. doi:10.1016/j.coldregions.2017.11.011

Zhuang, M., Gao, W., Zhao, T., Wei, Y., and Shao, H. (2021). Mechanistic investigation of typical loess landslide disasters in Ili Basin, Xinjiang, China. *Sustainability–Basel* 13, 635. doi:10.3390/su13020635